INVESTIGATION OF THE MICROSTRUCTURE OF FRACTURE SPECIMENS FROM FIVE DIFFERENT PLATES OF THE 500 KG PROGRAM HEAT OF V-4CR-4TI. -- E.G. Donahue, G.R. Odette, G.E. Lucas (University of California, Santa Barbara)

OBJECTIVE

The objective of this study was to determine and compare microstructures of five plates of V-4Cr-4Ti that have been used to obtain fracture toughness and tensile data in a program to develop fracture assessment methods.

SUMMARY

Four of the five plates of V-4Cr-4Ti had similar microstructures. They exhibited banding of Ti-OCN particles, which were distributed in planar arrays parallel to the rolling plane. The grain sizes were reduced in the vicinity of the particles. The plates differed in the size reduction of these grains and the thickness and spacing of the bands. The fifth plate had a more uniform distribution of Ti-OCN particles and no evidence of bands of reduced-size grains. The microstructures are considered in relation to fracture behavior.

PROGRESS AND STATUS

Introduction

We have undertaken an effort to understand the mechanisms of fracture in vanadium-based alloys and to develop fracture assessment methods for structures comprised of vanadium alloys [1,2]. As part of this effort, we have been testing unirradiated and irradiated fracture specimens of V-4Cr-4Ti alloys [1-4]. However, the specimens have been fabricated from various plates produced from the 500 kg program heat of V-4Cr-4Ti, and differences in fracture behavior have been found between various batches of specimens made from the different plates. This is believed to be due to microstructural differences. An inhomogeneous distribution of titanium-oxycarbonitrides (Ti-OCN) often forms in the solid solution matrix of V-Cr-Ti alloys during thermo-mechanical processing [5,6] The formation of these precipitates can be significant since they have been shown to influence the fracture behavior of V-Cr-Ti alloys by removing interstitial elements from the matrix [7]. Therefore, in order to compare fracture data from different plates of this heat of V-4Cr-4Ti, it is necessary to know what, if any, differences exist in the microstructure and distribution of precipitates exist.

While some microstructural investigations have been conducted on this heat at ORNL [5], there has been no comprehensive metallographic study of all the fabrication products of this heat. Hence, we have undertaken an effort to augment the existing microstructural data, and work to date is presented here.

Experiment

Material from fracture specimens machined from plates of the 500 kg program heat of V-4Cr-4Ti was used to investigate the microstructural differences among the plates. The plates were M150, Q250, Q150, V250, and V150, as identified by Oak Ridge National Laboratory (ORNL) [5]. Table 1 summarizes the relationship between ORNL and Argonne National Laboratory (ANL) identification codes and the final plate thicknesses. The plates were all prepared by Teledyne Wah Chang, Albany (TWCA) from parent stock of plate V250, which was fabricated by warm rolling a rectangular extrusion in the extrusion direction to 6.35 mm, with intermediate 1050°C/2h vacuum anneals. The subsequent steps in producing the other plates are shown in Schematic 1. All of the anneals shown in Schematic 1 were performed at TWCA. Subsequent to plate fabrication, 1/3-sized Charpy V-notch (MCVN) and compact tension (CT) specimens were machined from the plates, and the specimens were then vacuum annealed at ORNL for 2h at 1000°C. For all plates this was done to remove any hydrogen picked up during machining. For plates V150 and Q150 this also served as a recrystallization anneal following the previous warm roll.

Samples of material from each plate were derived from the broken halves of the MCVN specimens following testing. Samples were mounted for metallography in each of three orientations: view plane parallel to the rolled surface (LT), view plane orthogonal to the rolling direction (TS), and view plane orthogonal to the transverse direction (LS), as described in ASTM-E3 [8]. Sample orientations are illustrated in Figure 1. Mounted samples were ground and polished through 0.05 μm alumina and etched using a solution of 10% HF, 30% HNO_3, and 60% H_2O applied to the samples with a cotton swab for four minutes. An optical metallograph was used to inspect the etched surfaces for grain boundaries and inclusion distribution patterns. Samples were also inspected with a JEOL 6300F scanning electron microscope (SEM).

Table 1. Summary of the plate identification codes and thicknesses.

ORNL I.D.	ANL I.D.	Thickness (mm)
V250	Plate D	6.4
Q250	Plate A, Ann.	6.4
Q150	—	3.8
M150	Plate A	3.8
V150	Plate DD	3.8

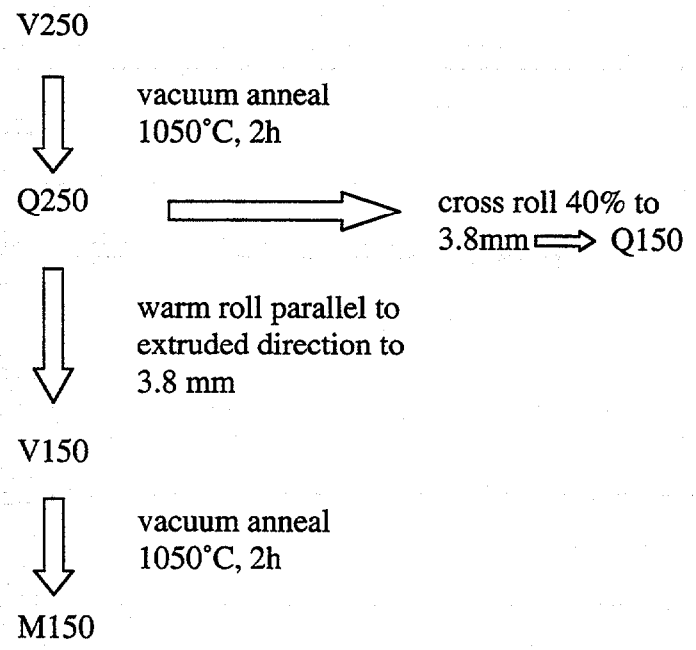

Schematic 1. Processing histories for plates

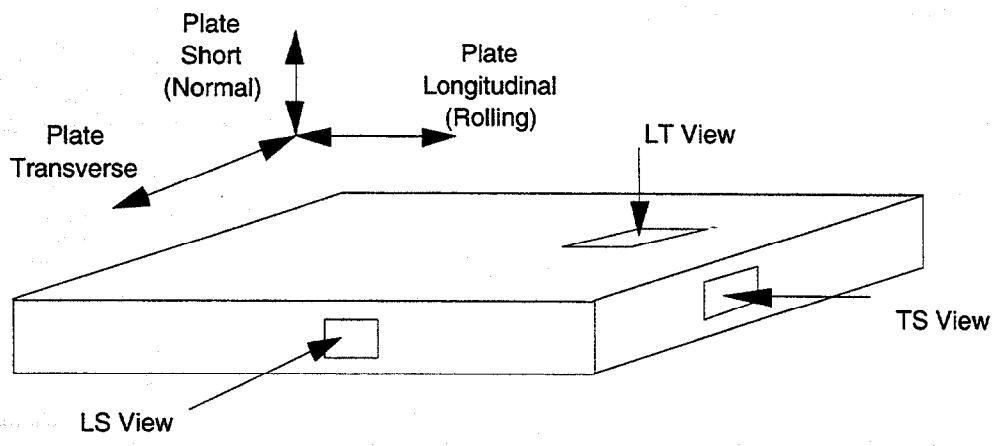

Figure 1. Diagram of the plate directions and views used in metallography.

Results

Figure 2 shows the optical micrographs of the etched samples from V250 in each of the three orientations at low- and higher- magnification. The LT view (a and b) of the V250 sample shows generally uniform grain sizes of 25 – 50 μm in diameter. The TS (c and d) and LS (e and f) views are characterized by bands of particles throughout the thickness of the plate. The particles are presumed to be Ti-OCN precipitates. The bands are typically 25 – 100 μm thick and extend as roughly planar arrays parallel to the rolling plane. Within the particle-rich regions grains are smaller resulting in a bimodal grain-size distribution of alternating coarse- and fine-grained regions through the plate thickness. Grain sizes in the banded, finer grain regions are typically 10 – 20 μm in diameter; grains in the coarse regions are typically 25 – 50 μm in diameter. The bands of finer grains are typically 20 – 30 μm thick and 75 – 100 μm apart.

Figure 3 shows the LT (a and b), TS (c and d), and LS (e and f) views of the Q250 plate. The Q250 plate has a microstructure very similar to that of V250. The LT view shows uniform grain sizes of ~25 μm diameter. The LS and TS views show the banding and the associated course (25 – 50 μm diameter) and fine (10 – 20 μm diameter) grain regions. The bands of finer grains are typically 25 – 50 μm thick and 100 – 125 μm apart. The banding appears to be somewhat more severe, and the bands thicker than in the V250 plate.

Figure 4 a and b show the LT view of Q150 material at low- and higher-magnification; in this view the grains are uniform in size, ~25 μm diameter, similar to V250 and Q250. There are also particle-rich bands in this plate, as shown in Figure 4 in the TS (c and d) and LS (e and f) views. However, there is less severe banding and reduction of grain sizes associated with the banded Ti-OCN particle distribution than in Q250. The bands of finer grains are typically thin, ~25 μm, compared to the Q250 plate; and they are ~50 μm apart.

Figure 5 shows the optical micrographs of the etched samples from M150 in each of the three orientations at low- and higher- magnification. The LT view (a and b) of the M150 sample shows generally uniform grain sizes of 25 – 50 μm in diameter. The TS (c and d) and LS (e and f) views are characterized by bands of particles typically 25 – 100 μm throughout the thickness of the plate. Grain sizes in the banded, finer grain regions are typically 10 – 20 μm in diameter; grains in the coarse regions are typically 25 – 50 μm in diameter. The bands of finer grains are typically 50 – 100 μm thick and 100 – 125 μm apart. The structure is quite similar to that observed in Q250.

Figure 6 shows optical micrographs of V150. As in the other plates, in the LT view (6 and b) the grains are uniform in size (~25 μm diameter). However, unlike the other plates, V150 does not exhibit the well-defined banding in the TS (6 c and d) or LS (6 e and f) views, but similar and relatively uniform grain sizes.

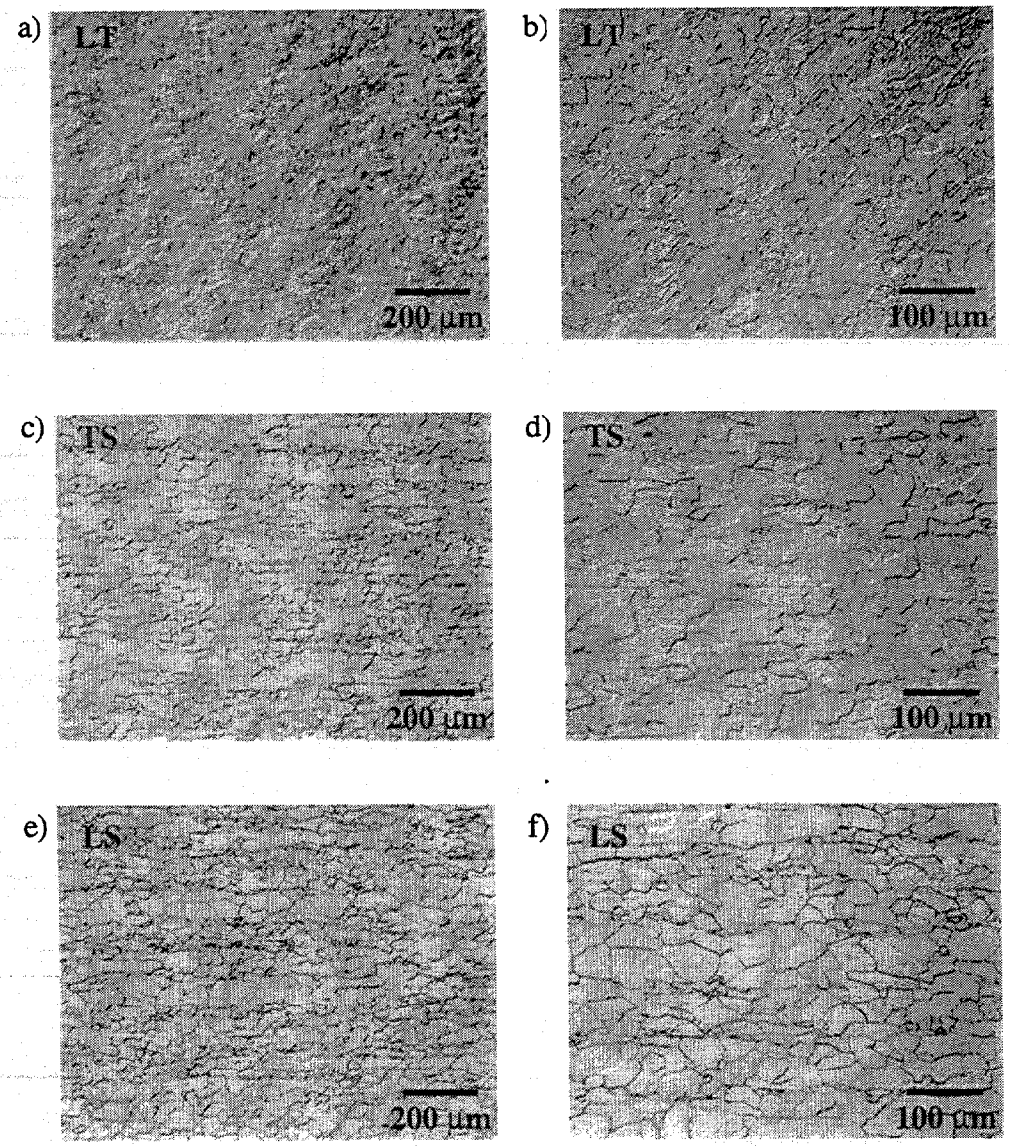

Figure 2. Low- and higher-magnification optical micrographs of V250. The LT view (a and b) shows uniform grain sizes while the TS (c, d) and LS (e, f) views show a banded grain size distribution associated with a non-uniform, banded distribution of particles.

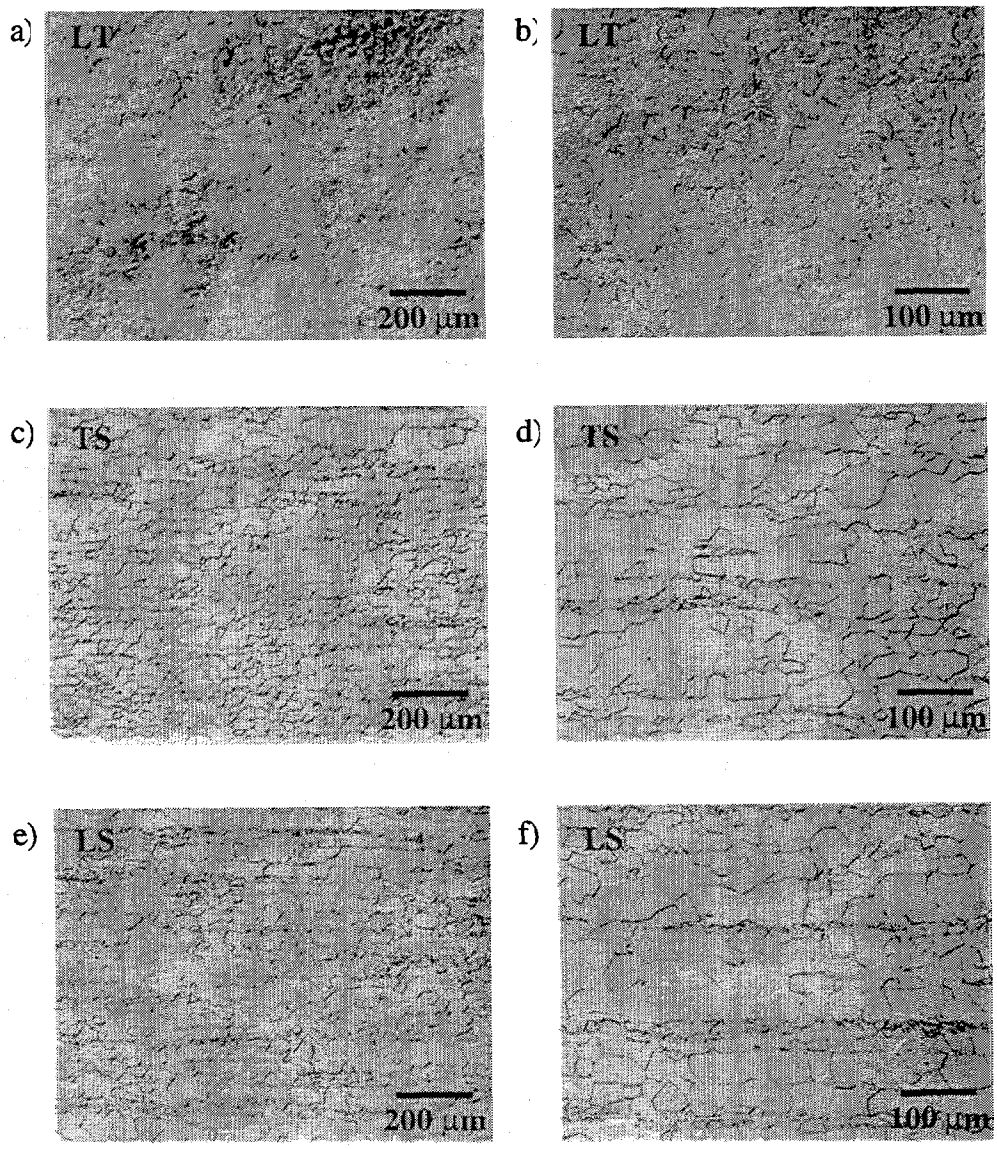

Figure 3. Low- and higher-magnification optical micrographs of Q250. The LT view (a and b) shows uniform grain sizes while the TS (c, d) and LS (e, f) views show a banded grain size distribution associated with a non-uniform, banded distribution of particles, similar to that in V250, but slightly more severe.

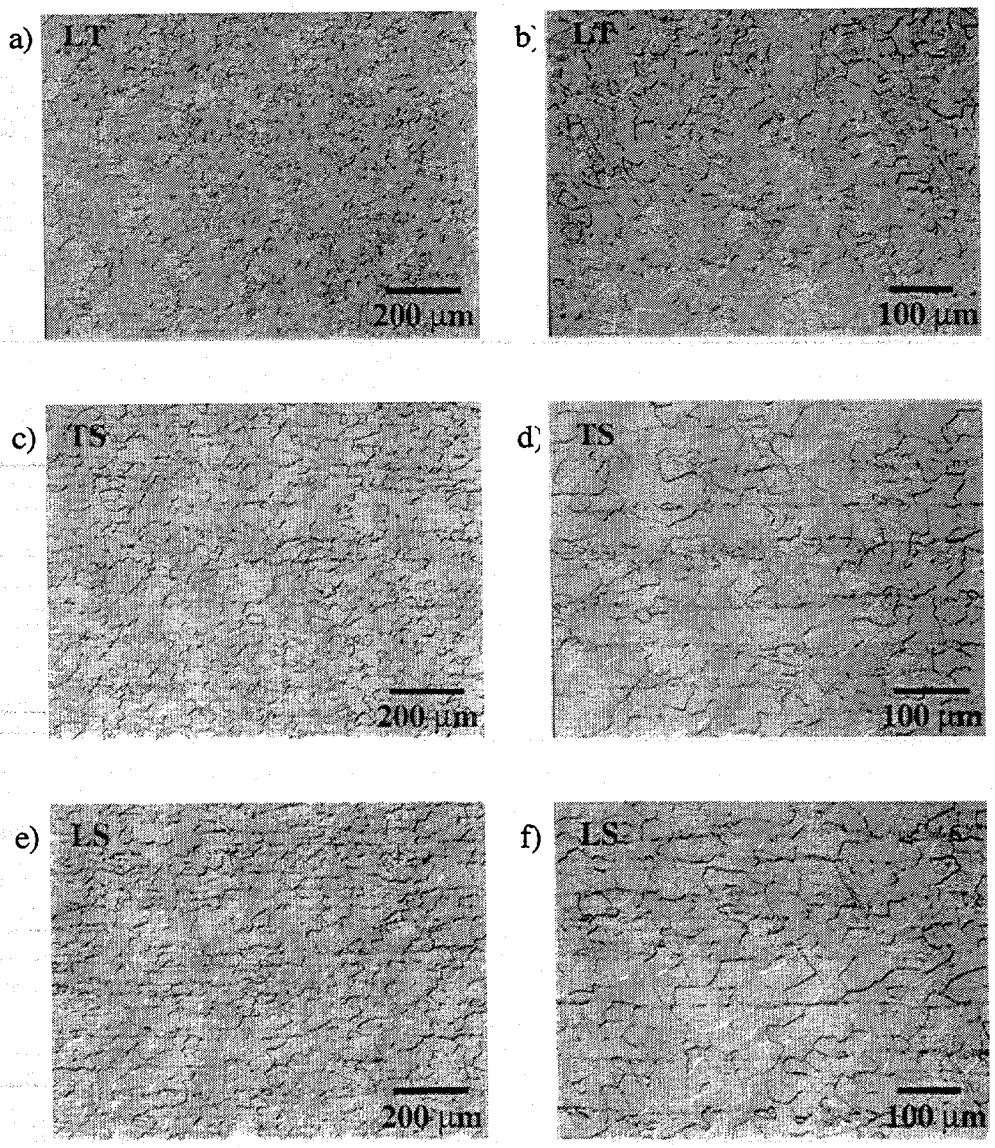

Figure 4. Low- and higher-magnification optical micrographs of Q150. The LT view (a and b) shows homogeneous grain size distribution while the TS (c and d) and LS (e and f) views show banding of Ti-OCN particles, but a much less pronounced reduction of grain sizes in the bands than seen in Q250.

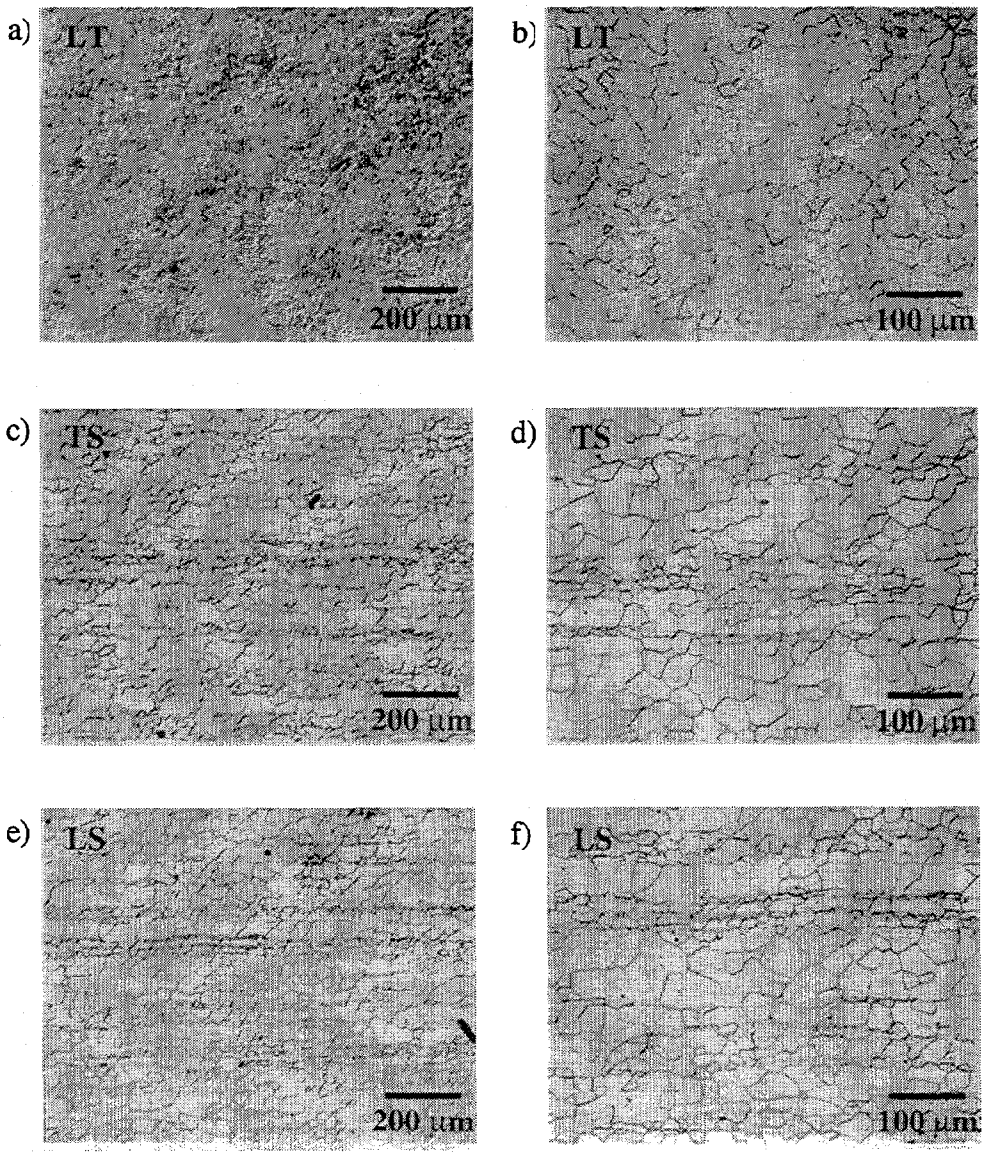

Figure 5. Low- and higher-magnification optical micrographs of M150. The LT view (a, b) shows uniform grain sizes while the TS (c, d) and LS (e, f) views show a banded grain size distribution associated with a non-uniform, banded distribution of particles. The banding is more severe than in Q150, and is similar to that seen in Q250.

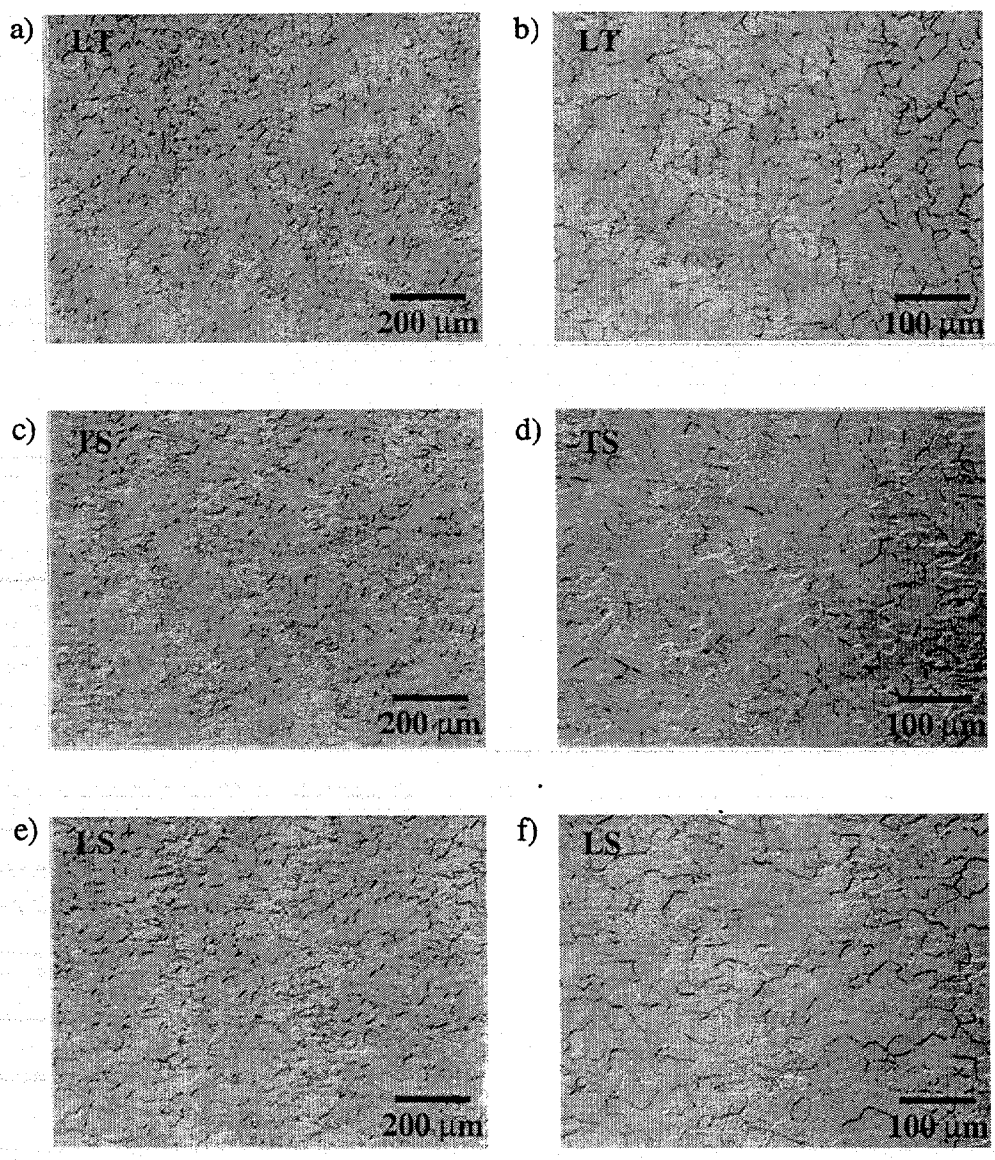

Figure 6. Low- and higher-magnification optical micrographs of V150. The LT view (a, b) shows a homogeneous grain size distribution, as in the other four plates. However, the TS (c and d) and LS (e and f) views show a much more uniform distribution of Ti-OCN particles and, consequently, a much more uniform grain size distribution than in the other plates.

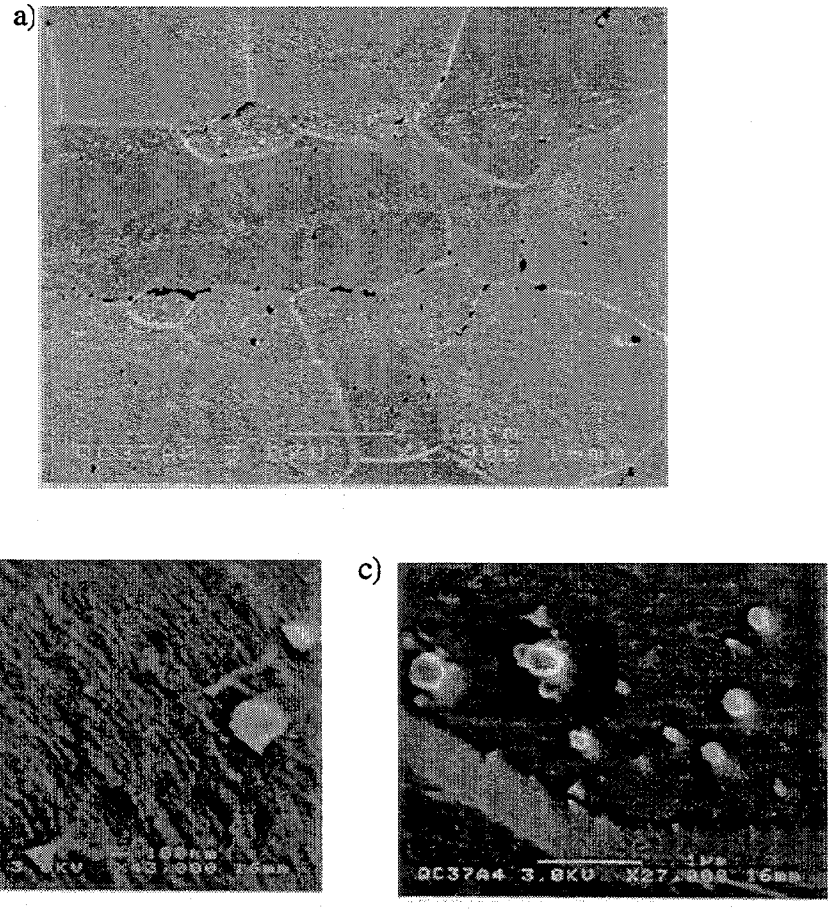

Figure 7. SEM micrographs of the LT view of Q250 showing: a) a region of small grains in the vicinity of Ti-OCN particles which are in a band from left to right: b) and c) high magnification micrographs of representative particles in this region.

SEM micrographs of the TS view of a representative sample from plate Q250 are presented in Figure 7. Figure 7a shows a region of small grains in the vicinity of the particles, and higher magnification images of the Ti-OCN particles are shown in Figure 7 b and c. The Ti-OCN particles range in size from ~0.1 to 0.3 μm. The structure and content of these particles was analyzed by Hoelzer at ORNL, who determined that they are based on the fcc TiC phase with O and N in solid solution.

Discussion

A summary of metallography results is given in Table 2. Metallography on plates Q250, Q150, and M150 has been reported previously [5], and the results are in general agreement with the findings here. All plates had similar bulk, equiaxed grain sizes in the range 25 – 50 μm, but differed in the extent of banding and the size and number of the

small grains in the bands. Plates V250 and Q250 had similar processing histories and microstructures. The extra high-temperature anneal at 1050°C for 2h for Q250 appeared to have little affect on the microstructure. The additional cross roll given to plate Q150 appeared to decrease the band spacing and thickness. However, the additional reduction given to plate M150 (compared to plate Q250) appeared to have little effect on the band spacing; and indeed, the band thickness appeared to be somewhat larger. Finally, the microstructure of V150 was quite different than M150, even though both plates received the same reduction and M150 received an additional vacuum anneal after specimen fabrication.

Table 2. Summary of metallography results.

Plate I.D.	Degree of Banding	Grain Diameters (μm) Bulk	Band	Band Spacing (μm)	Band Thickness (μm)
V250	Moderate	25-50	10-20	75-100	0-25
Q250	Moderate	25-50	10-20	100-125	25-50
Q150	Slight	25-50	10-20	50	25
M150	Severe	25-50	10-20	100-125	50-100
V150	None	25-50	—	—	—

It has been previously suggested that the Ti-OCN precipitates during extrusion when the temperature falls below 1125°C; and because of temperature variation throughout the extrusion, the precipitates are inhomogeneously distributed throughout the extrusion [5]. The precipitate clusters appear to flatten in the rolling plane during warm rolling. Intermediate anneals after warm rolling result in recrystallization; but the precipitates do not dissolve, and their presence hinders grain growth — hence the bimodal grain size distribution. The difference between V150 and M150 is probably due to this inhomogeneous distribution of Ti-OCN — plate M150 coming from a piece of the extrusion that fell below 1125°C, and plate V150 coming from a piece that largely remained above 1125°C. Since only limited sampling was done in this study, the degree to which these microstructures represent the entire plate is not known at this time.

Figures 8 and 9 show plots of effective toughness versus temperature obtained on several of these plates and reported previously [1–4]. Figure 8 shows effective toughness-temperature curves for the Q250 (Figure 8a) and Q150 (Figure 8b) plates obtained from MCVN specimens with the crack plane parallel to the TS view. Hence, the planes of the bands of precipitates and small grains would lie orthogonal to the crack plane and parallel to the crack direction. Both plates exhibit fracture by cleavage pop-ins (open circles) at the lower temperatures and stable crack growth (open squares) at the higher temperatures. The transition temperature delineating this behavior is about -160°C for the Q250 plate and about -180°C for the Q150 plate. Since the banding was somewhat smaller in the Q150 plate, this may play a role in the lower transition temperature.

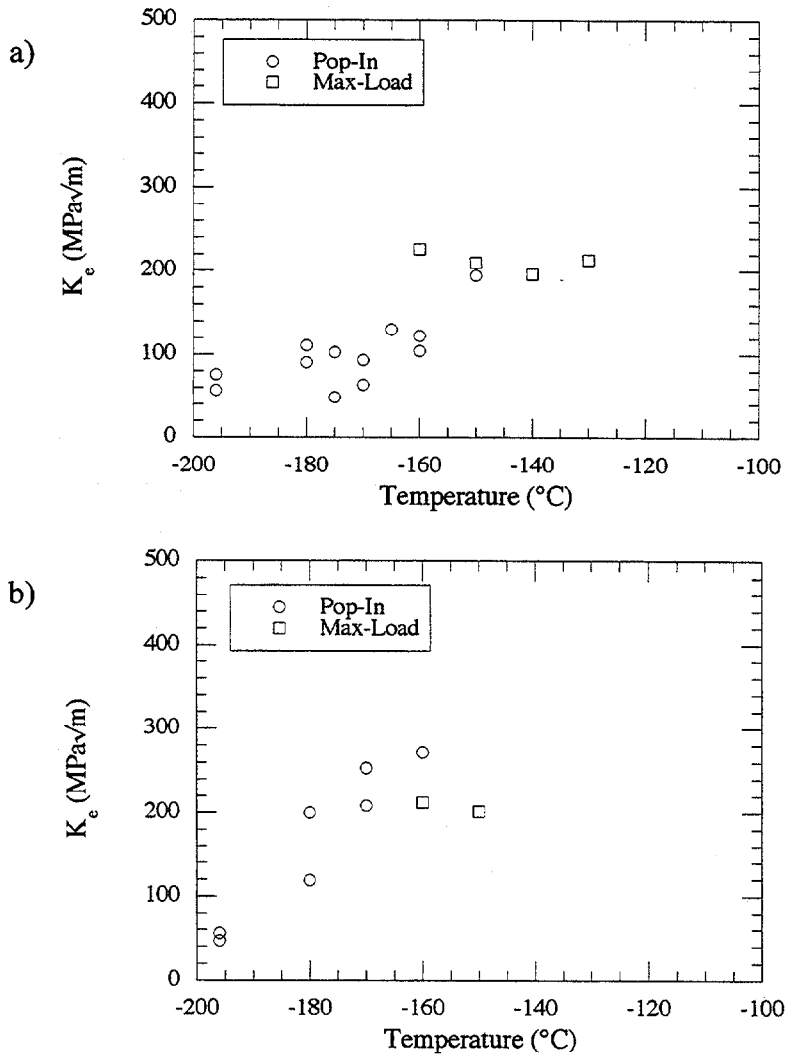

Figure 8. Effective toughness temperature curves for a) Q250 and b) Q150.

Figure 9 shows the effective toughness temperature curves for plates V250 (Figure 9a) and V150 (Figure 9b). The data for V250 were obtained from 0.26T CT specimens and the data for V150 were obtained from 0.16/0.26T CT specimens (0.26T CT in all dimensions except thickness which was 0.16T) as well as pre-cracked 0.16T 3-point bend specimens. In both cases, specimens were tested in two orientations: one in which the crack plane ran parallel to the TS view (LT orientation) and one in which the crack plane ran parallel to the LS view (TL orientation). In both cases, the planes of the bands of precipitates and small grains would lie orthogonal to the crack plane and parallel to the crack direction. Again the material exhibits fracture by cleavage pop-ins at lower temperatures transitioning to stable ductile fracture at the higher temperatures. For both

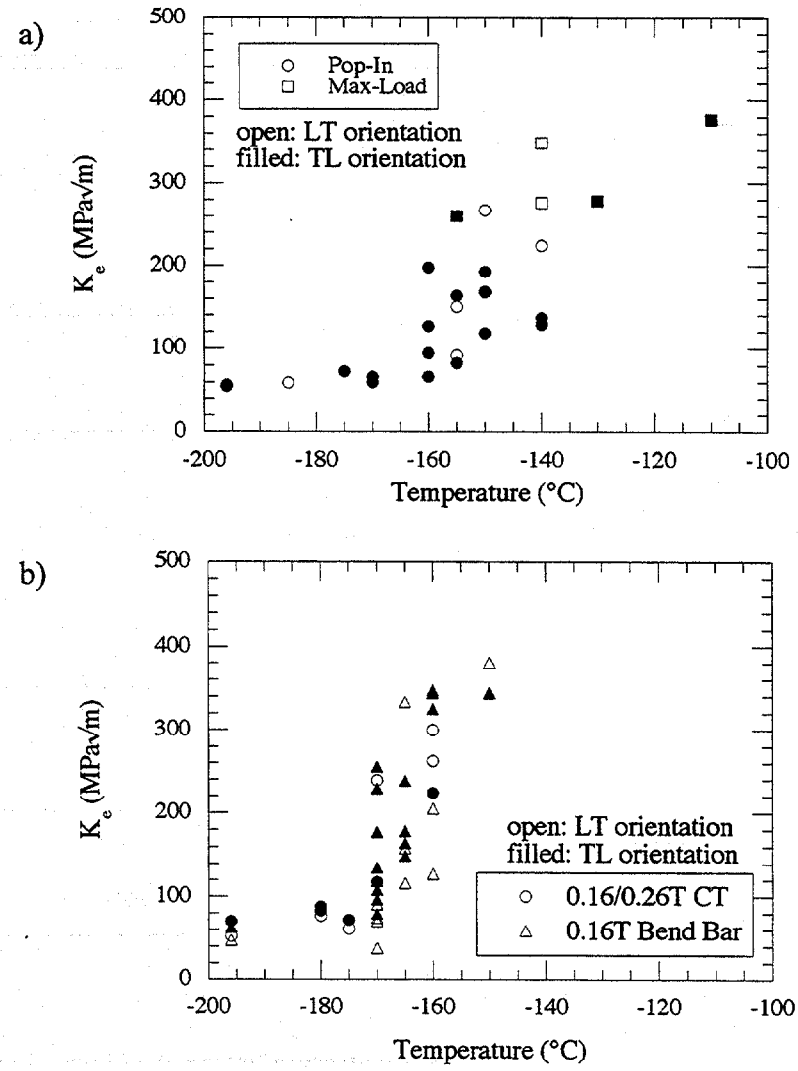

Figure 9. Effective toughness-temperature curves for a) V250 and b) V150.

V250 and V150 there is little effect of specimen orientation, consistent with the similar microstructures observed in the TS and LS views. For V150 there was also little difference in the data obtained for the two specimen types. The Q250 data show a transition temperature of roughly -150°C, while the V150 data show a sharper transition at about -165°C. Again the lower transition temperature seems to correlate with the lesser degree of banding and smaller density of visible Ti-OCN in the V150, although the thinner specimens for this data set currently confound this comparison.

Cleavage fracture in V-4Cr-4Ti is believed to occur by the nucleation of numerous cleavage microcracks ahead of the loaded crack, which coalesce and propagate as an unstable macrocrack when a critical area A* ahead of the crack is stressed above a

critical value σ^* [1-2]. Cleavage microcracks can be nucleated by brittle particles, and the magnitude of σ^* can scale inversely with the size of the trigger particles. Hence, a larger trigger particle density could increase the temperature for the transition from ductile to brittle cleavage fracture. This suggests that the large Ti-OCN particles may play a direct role in cleavage fracture, and hence control of these particles may improve the fracture behavior.

FUTURE WORK

Scanning electron microscopy will be performed to look for direct evidence of Ti-OCN particle affiliation with cleavage microcracking. Since only limited metallographic sampling was performed here, and since it is apparent that different plates can have significantly different microstructures, it is important that continued systematic microstructual investigations be pursued in the fusion program.

REFERENCES

1. Odette, G. R., Lucas, G. E., Donahue, E., Sheckherd, J. W., *J. Nucl. Mater.*, 233-237 (1996) 502-506.

2. Odette, G. R., Donahue, E., Lucas, G. E., Sheckherd, J. W., Effects of Radiation on Materials: 18th International Symposium, ASTM-STP-1325, American Society for Testing and Materials (1999) 1089-1108.

3. E.G. Donahue, G.R. Odette, G.E. Lucas, *Fusion Materials Semiannual Progress Report*, DOE/ER-0313/27 (2000)

4. E.G. Donahue, G.R. Odette, G.E. Lucas, *Journal of Nuclear Materials*, in Press.

5. A. F. Rowcliffe, D. T. Hoelzer, *Fusion Materials Semiannual Progress Report*, DOE/ER-0313/25 (1999) 42.

6. D.T. Hoelzer, *Fusion Materials Semiannual Progress Report*, DOE/ER-0313/25 (1999) 59.

7. S.J. Zinkle, H. Matsui, D.L. Smith, A.F. Rowcliffe, E. van Osch, K. Abe, V.A. Kazakov, *Journal of Nuclear Materials*, 258-263 (1998) 205.

8. "Standard Practice for Preparation of Metallographic Specimens," ASTM E3, *Annual Book of ASTM Standards vol, 3.01*, (1998).